ChemPlusChem

Research Article
doi.org/10.1002/cplu.202300523

Chemistry Europe
European Chemical Societies Publishing

www.chempluschem.org

Halide Complexes of 5,6-Dicyano-2,1,3-Benzoselenadiazole with 1:4 Stoichiometry: Cooperativity between Chalcogen and Hydrogen Bonding

Ekaterina A. Radiush,[a] Hui Wang,*[b] Elena A. Chulanova,[a, c] Yana A. Ponomareva,[a, d] Bin Li,[b] Qiao Yu Wei,[b] Georgy E. Salnikov,[a] Svetlana Yu. Petrakova,[a] Nikolay A. Semenov,*[a] and Andrey V. Zibarev[a]

The $[M_4{-}Hal]^-$ (M = the title compound; Hal = Cl, Br, and I) complexes were isolated in the form of salts of $[Et_4N]^+$ cation and characterized by XRD, NMR, UV-Vis, DFT, QTAIM, EDD, and EDA. Their stoichiometry is caused by a cooperative interplay of σ-hole-driven chalcogen (*ChB*) and hydrogen (*HB*) bondings. In the crystal, $[M_4{-}Hal]^-$ are connected by the π-hole-driven *ChB*; overall, each $[Hal]^-$ is six-coordinated. In the *ChB*, the electrostatic interaction dominates over orbital and dispersion interactions. In UV-Vis spectra of the M + $[Hal]^-$ solutions, *ChB*-typical and $[Hal]^-$-dependent charge-transfer bands are present; they reflect orbital interactions and allow identification of the individual $[Hal]^-$. However, the structural situation in the solutions is not entirely clear. Particularly, the UV-Vis spectra of the solutions are different from the solid-state spectra of the $[Et_4N]^+[M_4{-}Hal]^-$; very tentatively, species in the solutions are assigned $[M{-}Hal]^-$. It is supposed that the formation of the $[M_4{-}Hal]^-$ proceeds during the crystallization of the $[Et_4N]^+[M_4{-}Hal]^-$. Overall, M can be considered as a chromogenic receptor and prototype sensor of $[Hal]^-$. The findings are also useful for crystal engineering and supramolecular chemistry.

Introduction

Secondary bonding interactions (SBIs),[1–4] also called noncovalent interactions, are important for fundamental chemistry and its multidisciplinary applications.[5–16] One of the most interesting applications of SBIs is ion recognition, sensing, and transport by neutral compounds; and anion recognition and sensing are more challenging than those of cations.[4,7–12,17–19,20] Amongst anions, halides $[Hal]^-$ (Hal = F, Cl, Br, I) are essentially important for living beings and their environment.[19]

Amongst SBIs used for anions recognition and sensing, hydrogen,[21–23] halogen[24–31] and chalcogen[26,29–48] bondings (*HB*, *XB* and *ChB*, respectively), are, perhaps, the most important;[29,42] in the case of chalcogens, they embrace also hypervalent derivatives, e.g. EF_5 (E = S, Se, Te).[49] Combination of anion- and cation-receipting moieties in a single scaffold is possible to provide cooperative ion-pair recognition.[30,50]

Generally, SBIs contain contributions from electrostatic, orbital and dispersion interactions. The electrostatic interactions are associated with electrophilic areas at atoms in molecules. In molecular electrostatic potential (MEP) theory such areas arising from the anisotropy of the atomic charge distributions and corresponding to MEP positive values, are termed σ- and π-holes. The σ-holes are spatially located on the outer-side extensions of the σ-bonds, and π-holes are placed above and below the molecular plane. Due to this, the hole-based SBIs are highly directional.[1,35,51–62] In SBIs with anions σ-holes are mainly involved.[35,59,63–66]

Orbital contribution into *ChB* aligns with the well-established Alcock model[1] as an overlap of guest anion's unshared *n*-MO with σ*-MO of the chalcogen-containing host accompanied by donation of the electron density (charge transfer-CT) from the guest onto the host, *i.e.*, by their negative hyperconjugation.[67] Dispersion contribution is associated with high atomic polarizability of heavier atoms[68] in the host (*i.e.*, Se and Te) and guest molecules.

Thermodynamics of anion binding by *ChB* suggests that both enthalpy and entropy are important, and that its affinity and selectivity are controlled by a subtle interplay between *ChB* host, anion guest and solvent.[69,70] Importantly, *ChB* are redox-switchable, which can be used in anion recognition and sensing.[71]

Amongst recently recognized anion receptors, chromogenic/fluorogenic 1,2,5-chalcogenadiazoles (chalcogen = S, Se, and Te) and their fused derivatives should be highlighted. Their

[a] E. A. Radiush, Dr. E. A. Chulanova, Y. A. Ponomareva, Dr. G. E. Salnikov, S. Y. Petrakova, Dr. N. A. Semenov, Prof. Dr. A. V. Zibarev
Institute of Organic Chemistry
Siberian Branch, Russian Academy of Sciences
630090 Novosibirsk (Russia)
E-mail: klaus@nioch.nsc.ru

[b] Prof. Dr. H. Wang, B. Li, Q. Y. Wei
School of Physical Science and Technology
Southwest Jiaotong University
610031 Chengdu (P. R. China)
E-mail: wanghui@swjtu.edu.cn

[c] Dr. E. A. Chulanova
Current address: Institute for Applied Physics
University of Tübingen
72076 Tübingen (Germany)

[d] Y. A. Ponomareva
Department of Natural Sciences
National Research University – Novosibirsk State University
630090 Novosibirsk (Russia)

Supporting information for this article is available on the WWW under https://doi.org/10.1002/cplu.202300523

ChB-bonded complexes with anions (mostly halides), as well as with neutral Lewis bases, are characterized by XRD, UV-Vis, NMR, and quantum chemical calculations; in some cases, double *ChB* is observed to be based on simultaneous participation of two σ-holes at the same chalcogen atom.[51,72–92] The capacity of chalcogenadiazoles for the formation of *ChB* increases with the atomic number/polarizability[68] of the chalcogen. The common structural peculiarity of the complexes is that the *ChB* is longer than the sum of the covalent radii of the involved atoms but shorter than the sum of their van der Waals (VdW) radii, which directly indicates an orbital contribution.[72–81] In the form of crown ether-annulated derivatives,[88,93] chalcogenadiazoles have potential for cooperative ion-pair recognition. In crystalline chalcogenadiazolium salts,[94–96] cations and anions are connected by *ChB*.

In this work, novel $[\mathbf{1}_4{-}Hal]^-$ (**1** = 5,6-dicyano-2,1,3-benzoselenadiazole, Scheme 1; Hal = Cl, Br, and I, and F[73,97–100] is not involved) complexes are prepared, isolated in the form of $[Et_4N]^+[\mathbf{1}_4{-}Hal]^-$ salts and structurally defined by a number of techniques encompassing XRD. The unprecedented 4 : 1 stoichiometry of the complexes is caused by the cooperative interplay of two σ-hole-driven *ChB*s and two *HB*s; in the crystal, $[\mathbf{1}_4{-}Hal]^-$ are connected by a longer *ChB*s driven by the π-holes at **1** and each $[Hal]^-$ is six-coordinated. The structural situation in solution is not entirely clear. One can think that the formation of $[\mathbf{1}_4{-}Hal]^-$ proceeds during the crystallization of $[Et_4N]^+[\mathbf{1}_4{-}Hal]^-$ from solutions assumingly containing $[\mathbf{1}{-}Hal]^-$.

4,7-Dicyano isomer of **1**, *i.e.*, compound **2**, which does not form isolable complexes with $[Hal]^-$ under the same conditions, and reference selenadiazoles **3**–**7** (Scheme 1) are also discussed.

Results and Discussion

Molecular electrostatic potentials

The MEPs of **1** and **2** reveal typical of 1,2,5-chalcogenadiazoles two equivalent σ-holes at the Se atoms. The value of the MEP maximum at the σ-hole, $V_{S,max}$, for **1** and **2** is significantly larger than for the archetypal compound **3**;[101,102] and for **1** $V_{S,max}$ is ~2 kcal mol^{-1} larger than for **2**. Besides, **1** and **2** possess π-holes at both 6- and 5-membered rings (and the holes at the 5-membered rings are slightly deeper), which are absent in **3**. These π-holes are associated with perturbation of the molecular π-systems by the CN substituents (*cf.* C_6H_6 and $C_6(CN)_6$).[65,103] The $V_{S,max}$ values at the π-holes are notably smaller than at the σ-holes; they are practically equal for 6-membered rings of **1** and **2**, and differ by ~1.3 kcal mol^{-1} for 5-membered rings. In contrast to **3**, $V_{S,max}$ at the H atoms of **1** and **2** is slightly positive due to the electron-withdrawing effect of the CN substituents as well as chalcogenadiazole moiety (Figure 1, Table 1). The MEPs of the Hal^- anions reveal minima whose $V_{S,min}$ magnitudes decrease in the Hal order Cl > Br > I corresponding to electronegativities.

Comparison with reference compounds **3**–**7**[72,104] suggests that $V_{S,max}$ values for the σ-holes of **1** and **2** are high enough for this series (Scheme 1, Table 1) whose members, e.g. **6**,[72] actually form *ChB*-bonded $[Hal]^-$ complexes; or, e.g. **7**, can form those with various charged and neutral Lewis bases according to theoretical estimations.[51,73,74,80,81,89,105,106] Despite electrostatics is not the only contribution in the *ChB*, and comparison of $V_{S,min}$ values is rather simplifying, the MEPs analysis suggests that compounds **1** and **2** are promising for the field. However, their $[Hal]^-$ complexes are expected to be weaker bound than those of compound **6**.[72] For compounds **3** and **5** with smaller $V_{S,max}$ values than for **1** and **2** complexation with $[Hal]^-$ was observed neither in solutions nor in the crystalline phases.[104]

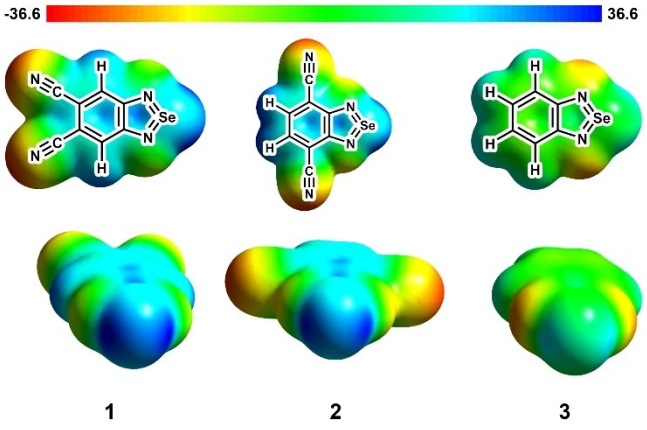

Figure 1. MEPs of selenadiazoles **1**–**3** in two perspectives from B3LYP/def2-tzvp calculations for isosurfaces with $\rho = 0.001$ a. u.

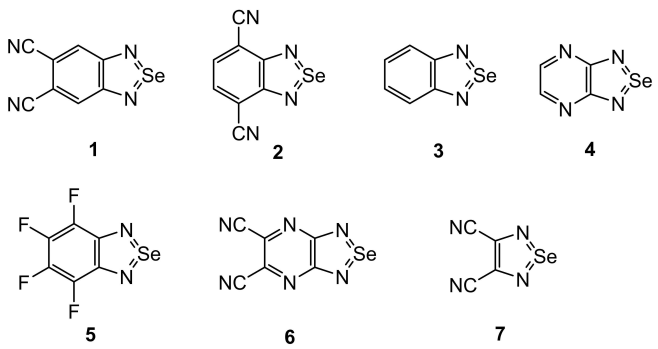

Scheme 1. Selenadiazoles **1**–**7**.

Table 1. B3LYP/def2-tzvp-calculated for isosurfaces with $\rho = 0.001$ a. u. $V_{S,max}$ of selenadiazoles **1**–**7** at σ- and π-holes and $V_{S,min}$ of $[Hal]^-$, kcal mol^{-1}.[a]

Compound	1	2	3	4	5	6	7
σ-hole	36.6	34.4	19.7	26.7	30.4	42.2	43.5
π_6-hole[b]	24.9	25.0	–	19.0	21.1	40.3	–
π_5-hole[c]	27.9	26.6	–	17.3	21.7	36.1	33.0
$[Hal]^-$	$[Cl]^-$		$[Br]^-$		$[I]^-$		
	−141.2		−132.7		−122.0		

[a] This work and refs.[62,72,93,101] [b] The π-hole at the 6-membered ring. [c] The π-hole at the 5-membered ring.

Solution situation and syntheses

For syntheses followed by XRD of the isolated products, $[Et_4N]^+[Hal]^-$ were used; whereas for spectral monitoring of the reaction mixtures, better soluble in organics (but possessing more structurally flexible cation) $[Bu_4N]^+[Hal]^-$ were applied (Hal = Cl, Br and I).

Slow evaporation of MeCN solutions of **1** with $[Et_4N]^+[Hal]^-$ (Hal = Cl, Br, I) in 1:1, 1:2, or 1:4 ratios of the starting materials invariably yields $[Et_4N]^+[\mathbf{1}_4{-}Hal]^-$ crystalline complexes featuring unprecedented[72–79] stoichiometry established by single-crystal XRD and suggesting *ChB* and *HB* participation (see Section 2.3).

Due to this unexpected result, the solution situation was studied in detail. UV-Vis monitoring of the reaction mixtures reveals that interaction of MeCN solutions of **1** and $[Bu_4N]^+[Hal]^-$ leads to the appearance of new long-wavelength bands in the UV-Vis area. The bands reveal typical $[Hal]^-$-depending bathochromic shift[72] allowing identification of the individual $[Hal]^-$ (Figure 2). However, high concentrations of **1** and $[Bu_4N]^+[Hal]^-$ are necessary to observe them. This indicates a rather weak interaction between **1** and $[Hal]^-$ implying that the corresponding equilibria are shifted towards **1**. The broadened solid-state UV-Vis spectra of the isolated $[Et_4N]^+[\mathbf{1}_4{-}Hal]^-$ differ from the spectra of the reaction mixtures of **1** with $[R_4N]^+[Hal]^-$ (R = Et, Bu) as they are markedly bathochromic-shifted (Figure 2). At switching from solution UV-Vis spectra to solid-state ones, band broadening is typical, however, for previously studied $[\mathbf{6}{-}Hal]^-$ (Hal = Cl, Br, I) the bands' maxima coincided fairly well in both incarnations.[72]

Dissolved in MeCN, the authentic $[Et_4N]^+[\mathbf{1}_4{-}Hal]^-$ reproduce UV-Vis spectra of the corresponding $\mathbf{1} + [Et_4N]^+[Hal]^-$ reaction mixtures (Figure 2).

Theoretical UV-Vis spectra of the isolated $[\mathbf{1}_4{-}Hal]^-$ and expected $[\mathbf{1}{-}Hal]^-$ were calculated by TD-DFT[108,109] for their optimized geometries (SI); the double-hybrid B2PLYP functional[110] was chosen as performing well for related compounds.[74,111] For $[\mathbf{1}{-}Hal]^-$, the calculations embraced both gas phase and MeCN solution with the conductor-like polarizable continuum model (C-PCM)[112] for the solvent, and for $[\mathbf{1}_4{-}Hal]^-$, a gas phase (SI). For $[\mathbf{1}_4{-}Hal]^-$, comparison of the solid-state (Figure 2) and theoretical (SI) UV-Vis spectra reveal that the calculations strongly underestimate energies of long-wavelength electronic transitions in a Hal-dependent way, which should be taken into account in discussing solution spectra of the reaction mixtures. Without this correction, calculated UV-Vis spectra of $[\mathbf{1}{-}Hal]^-$ correspond rather to the experimental solid-state spectra of the isolated $[Et_4N]^+[\mathbf{1}_4{-}Hal]^-$ than to the solution spectra of the reaction mixtures (Figure 2; SI). Particularly, measured/calculated λ_{max} (nm) of the longest-wavelength band is ~385/429, ~400/503, and 461/644 for Hal = Cl, Br and I, respectively; gas-phase calculated λ_{max} values are 399, 496 and 629 in the same order, *i.e.*, blue-shifted. In any way, a discrepancy between experimental UV-Vis spectra of the reaction mixtures and calculated spectra of $[\mathbf{1}{-}Hal]^-$ and $[\mathbf{1}_4{-}Hal]^-$ is much less for the $[\mathbf{1}{-}Hal]^-$. Therefore, taking into account previous results[72–86] and very tentatively, the $\mathbf{1} + [Hal]^- \leftrightarrow [\mathbf{1}{-}Hal]^-$ equilibrium (Scheme 2) can be assumed for the reaction mixtures, with the formation/synthesis of $[\mathbf{1}_4{-}Hal]^-$ occurring during crystallization of the isolated products employing *HB*. In this particular study, the conventional solution NMR and ESI-MS, which typically are reliable and informative,[40,72–74,76,78,104] yielded limited results. With variable-temperature ^{35}Cl and ambient-temperature ^{77}Se NMR, only the fact of interaction between **1** and $[Hal]^-$ in solution was confirmed; whereas with ESI-MS, no anionic complexes were detected (SI).

According to TD-DFT, the MOs involved in the lowest-energy electron excitations are spatially localized at the different areas of molecular scaffolds (SI), thus confirming the CT nature of the corresponding long-wavelength bands in the UV-Vis spectra (Figure 2); and for $[\mathbf{1}{-}Hal]^-$, the CT values are 0.16, 0.10 and 0.07 e for Hal = Cl, Br and I, respectively. It contradicts the electronegativities of Hal but is typical.[72] Within Alcock hyperconjugation model,[1] it can be tentatively explained by better overlap of the MOs involved in *ChB* in $[\mathbf{1}{-}Cl]^-$ as compared with $[\mathbf{1}{-}Br]^-$ and $[\mathbf{1}{-}I]^-$.

Mixtures of compound **2** with $[Et_4N]^+[Hal]^-$ (Hal = Cl, Br, I) in MeCN are also colored and reveal new long-wavelength bands (SI). As with **1**, high concentrations of $[Hal]^-$ are necessary to

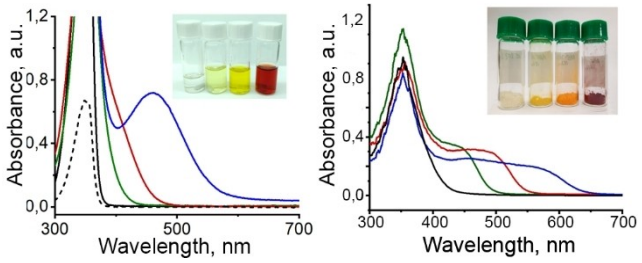

Figure 2. Left: Solution UV-Vis spectra of the individual **1** (4.33×10^{-5} M, dashed black line; 1.66×10^{-4}, solid black line; λ_{max}, nm/log ε: 354/4.18) and mixtures of **1** (1.66×10^{-4}, 1.99×10^{-4} and 3.34×10^{-4} M, respectively) with $[Et_4N]^+[Cl]^-$ (0.47 M, green line; λ_{max}, nm: ~385), $[Et_4N]^+[Br]^-$ (0.98 M, red line; λ_{max}, nm: ~400), and $[Et_4N]^+[I]^-$ (1.06 M, blue line; λ_{max}, nm/log ε: 461/3.73) in MeCN; for Cl and Br containing species, λ_{max} are very approximate, and log ε are not specified, due to the overlap of the spectral bands (SI). Right: Solid-state UV-Vis spectra of **1** (black line) and $[Et_4N]^+[\mathbf{1}_4{-}Hal]^-$ (Hal = Cl, green line; Br, red line; and I, blue line) in the form of the Kubelka-Munk function[107] of diffuse reflectance spectra. Inserts show the $\mathbf{1} + [Et_4N]^+[Hal]^-$ reaction solutions and the isolated $[Et_4N]^+[\mathbf{1}_4{-}Hal]^-$. Dissolving $[Et_4N]^+[\mathbf{1}_4{-}Hal]^-$ in MeCN provides spectra of the corresponding **1** $+ [Et_4N]^+[Hal]^-$ reaction mixtures (left).

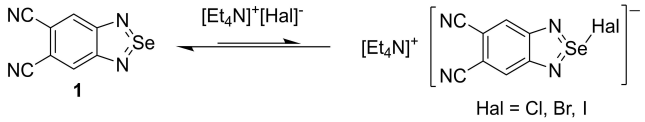

Scheme 2. Assumed 1:1 equilibrium of compound **1** and $[Et_4N]^+[Hal]^-$ in solution. With this model, spectrophotometric titration affords complex formation constant K_{eq} ($L\,mol^{-1}$) of ~17 for Hal = Cl, and ~0.5–0.6 for Hal = Br, I (SI); previously, K_{eq} of ~21 and ~15 $L\,mol^{-1}$ were reported for $[\mathbf{6}{-}Hal]^-$ with Hal = Cl and Br, respectively.[72] and 0.07 e for Hal = Cl, Br and I, respectively. It contradicts the electronegativities of Hal but is typical.[72] Within Alcock hyperconjugation model,[1] it can be tentatively explained by better overlap of the MOs involved in *ChB* in $[\mathbf{1}{-}Cl]^-$ as compared with $[\mathbf{1}{-}Br]^-$ and $[\mathbf{1}{-}I]^-$.

observe them; and for Hal = Cl and Br, these bands are not well-resolved. For Hal = I, the position and intensity of a new band are about the same as in the case of compound **1** (Figure 2; ESI) In attempted co-crystallization of compound **2** with $[Et_4N]^+$ $[Hal]^-$ (Hal = Cl, Br, I) under the same conditions as with **1**, however, only starting materials were recovered. It independently highlights the essential importance of *HB* (see Section 2.3) for the formation of isolated $[\mathbf{1}_4{-}Hal]^-$ for which solitary *ChB* is not enough.

XRD structures

Similar to Se…N catemeric **3**[100,113,114] and its TCNQ-fused derivatives[87,115] and N-bonded BR_3 complexes,[82] XRD crystal structure of **1** (Figure 3; SI) does not feature $[Se{\cdots}N]_2$ supramolecular dimers observed for many 1,2,5-selenadiazoles[51,82,86,91,101,102,116,119] (XRD structure of **2** was not solved due to twinning of available crystals). The $[E{\cdots}N]_2$ (E = S, Se, Te) *ChBs* are attractive and their total bond strength is greater than either *ChB* individually; and neither a pair of CN substituents in 1,2,5-chalcogenadiazole ring (*cf.* compound **7**) nor its benzo-annulation (*cf.* compound **3**) has much influence on those.[51]

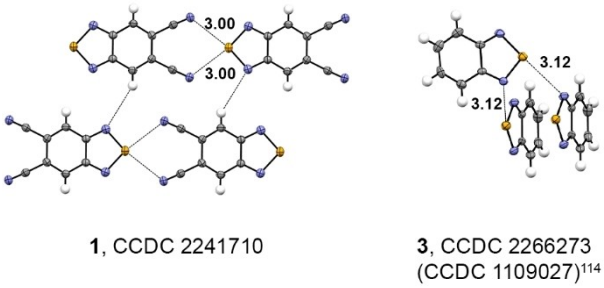

Figure 3. XRD structure of compounds **1** and **3** (ESI); dotted lines show SBIs (selected distances, Å). Color code: C–grey, H-light grey, N-blue, Se-orange.

Instead of the discussed $[Se{\cdots}N]_2$ dimers, the crystal structure of **1** reveals infinite head-to-tail chains with shortened Se…NC contacts of ~3.0 Å implying the formation of chelate via two Se…N *ChBs* between the Se atom of one molecule and both CN groups of the neighboring molecule; such ChBs are quite typical of CN-containing selenadiazoles.[87,115,120] These chains form layers by means of C–H…N(het) *HBs*; layers are π-stacked with the interplanar separation of ~3.4 Å. To some extent, this pattern resembles the crystal packing of **6** featuring shortened Se…NC contacts between the Se atom of one molecule and CN groups of two neighboring molecules.[120]

In the XRD structures of $[Et_4N]^+[\mathbf{1}_4{-}Hal]^-$ (Hal = Cl, Br, I) (Figure 4; SI), the $[Se{\cdots}N]_2$ dimers appear. With Hal = Cl and Br, $[\mathbf{1}_4{-}Hal]^-$ are almost planar, whilst in $[\mathbf{1}_4{-}I]^-$ two planar $\mathbf{1}_2$ dimers occupy planes intersecting at an angle of 43°. Each $[Hal]^-$ feature both in-plane and out-of-plane *ChBs*, within and between $[\mathbf{1}_4{-}Hal]^-$, respectively, and the latter are markedly longer than the former. The in-plane/out-of-plane *ChBs* of ~3.1/3.3, ~3.2/3.4 and ~3.4/3.8 Å for Hal = Cl, Br, and I, respectively, are by ~0.6/0.3, ~0.6/0.3, and ~0.5/0.1 Å shorter than the sums of the corresponding VdW radii (or constitutes 84/90, 85/91 and 87/98% of the VdW radii).[121,122] Taking into account their directionalities and distances, the in-plane bonds can be associated with σ-holes, and the out-of-plane bonds with π-holes, at **1**. The $[\mathbf{1}_4{-}Hal]^-$ feature the cooperative interplay of two σ-hole-based Se…$[Hal]^-$ *ChBs* with two C–H…$[Hal]^-$ *HBs* explaining the complexes' stoichiometry. The *HBs* involve the H atoms of **1** in the positions 4 and 7, and C–H…$[Hal]^-$ distance is ~3.0 Å for Hal = Cl, Br, and I.

This distance is comparable with the sums of the corresponding VdW radii.[121,122] Besides, in all structures, the neighboring $[\mathbf{1}_4{-}Hal]^-$ are connected by two π-hole-based Se…$[Hal]^-$ *ChBs*. Thus, each $[Hal]^-$ forms two σ- and two π-hole-based *ChBs*, and two *HBs*; and overall crystal structures feature a network of SBIs wherein individual complex anions $[\mathbf{1}_4{-}Hal]^-$ cannot be identified. A similar situation was previously observed for $[Et_4N]^+[\mathbf{6}_2{-}Cl]^-$ salt; notably, two surroundings of

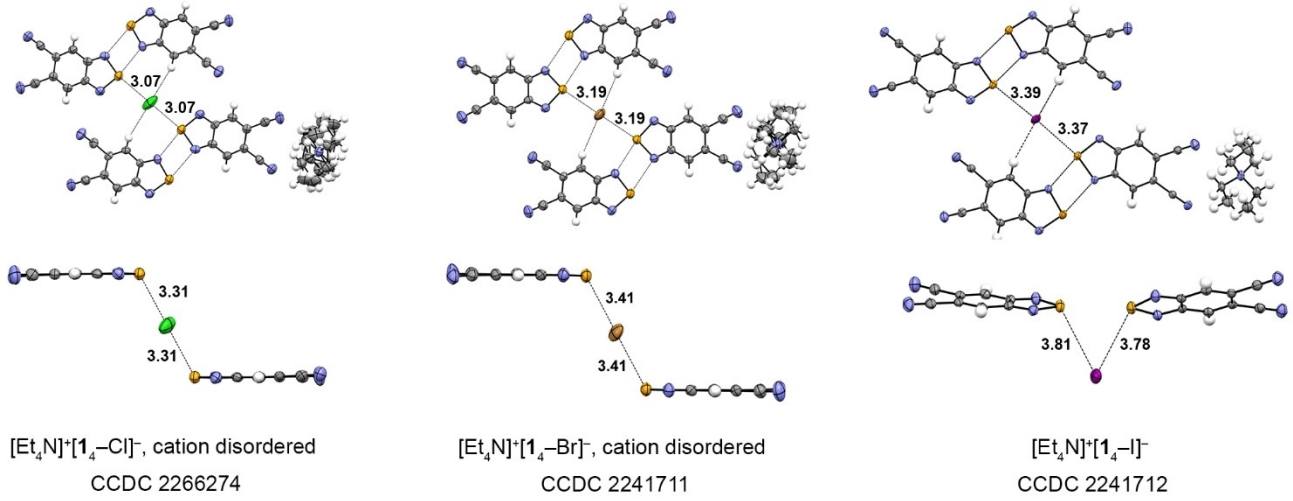

Figure 4. XRD structures of complexes $[Et_4N]^+[\mathbf{1}_4{-}Hal]^-$ (ESI); dotted lines show SBIs (selected distances, Å). Color code: C-grey, H–light grey, Br-brown, Cl-green, I-violet, N-blue, Se-orange.

$[Cl]^-$ in the crystal lattice revealed tetrafurcate and pentafurcate *ChB*.[72] For $[I]^-$, tetrafurcate bonding was found in its 1:2 complex with a triazole-based synthetic receptor.[19]

Previously, the actual or potential interplay of *ChB* with other SBIs, particularly *HB*, was discussed for 1,2,5-chalcogenadiazoles; and in some cases, they are rather competitive than cooperative.[4,30,31,102,123–125]

Structure and bonding of complex anions

Numerous complexes of 1,2,5-chalcogenadiazoles with anions assembled by *ChB* and featuring 1:1 and 1:2 stoichiometry are extensively characterized by various quantum chemical techniques before,[72–74,76–79,83,92,105,106] and this work is focused on the isolated $[\mathbf{1}_4{-}Hal]^-$. To study the bonding situation, DFT calculations and QTAIM, EDD, and EDA analyses were employed.

In a gas phase, $[\mathbf{1}_4{-}Hal]^-$ (Hal = Cl, Br, I) were optimized as minima on their respective PESs with B3LYP/def2-tzvp; the obtained structures are highly symmetric, which is in contrast to the asymmetric XRD structure with Hal = I (SI and Figure 5; $[\mathbf{1}_4{-}Hal]^-$ are divided into three interacting parts labeled as *I*, *II*, and *III*), with *I* and *II* consisting of two molecules of **1**, and *III* = $[Hal]^-$. In the optimized $[\mathbf{1}_4{-}Hal]^-$ (Figure 5), the *III*…Se distances increase in the Hal order Cl < Br < I as 2.99, 3.17, and 3.42 Å, respectively (Table 2), which match the XRD structures (Figure 4; SI) and agrees with the trend of the $V_{s,min}$ values of

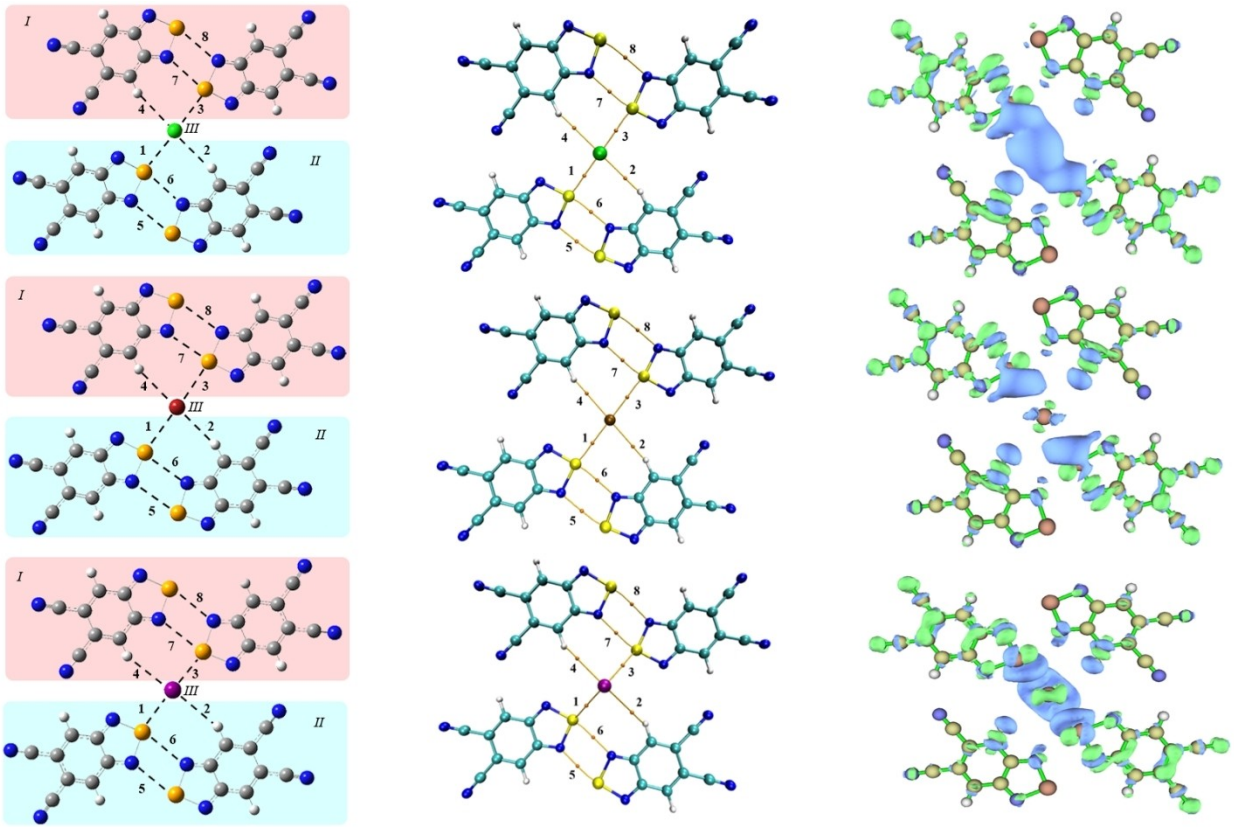

Figure 5. The bonding situation in $[\mathbf{1}_4{-}Hal]^-$; Hal = Cl, Br, and I are top-to-bottom. Left: The optimized B3LYP/def2-tzvp-structures featuring *I*, *II*, and *III* fragments (*I*, *II* consisting of two molecules of **1** *and III* = $[Hal]^-$) and shortened contacts 1–8 (for distances, see Table 2). Middle: QTAIM diagrams showing 1–8 bcp's (for properties, see Table 3). Right: The EDD maps with an equivalent value of 0.001 a. u.; the green area near the Se atoms and blue area near $[Hal]^-$ correspond to the main regions of increase and decrease of electron density, respectively (*cf.* similar areas near the H atoms). Color code: C-grey (left), aquamarine (middle) and light yellow (right), H–light grey, Br-brown, Cl-green, I-violet, N-blue, Se-orange (right) and yellow (middle).

Table 2. The E_{int} between fragments *I*–*III* in B3LYP/def2-tzvp-optimized $[\mathbf{1}_4{-}Hal]^-$, together with *d* distances of the shortened contacts.[a]

Hal	E_{int}, kcal mol^{-1}			*d*, Å							
	I↔*II*,*III*	*II*↔*I*,*III*	*III*↔*I*,*II*	1	2	3	4	5	6	7	8
Cl[b]	−20.67	−20.67	−53.74	2.99	3.11	2.99	3.11	3.12	2.96	2.96	3.12
Br[b]	−19.66	−19.67	−49.74	3.16	3.08	3.17	3.08	3.19	2.98	2.98	3.19
I	−7.56	−7.29	−34.51	3.43	3.49	3.42	3.49	3.03	3.05	3.06	3.02

[a] *III* = $[Hal]^-$; for shortened contacts *d*, see Figure 5. [b] Due to the high symmetry of $[\mathbf{1}_4{-}Hal]^-$, the *I*↔*II*,*III* and *II*↔*I*,*III* interaction energies are very close and match after rounding to two decimal places.

the $[Hal]^-$ (Table 1). The *III*…H distances are 3.11, 3.08, and 3.49 Å, respectively; for Hal = I, they are pretty different from the XRD values of 3.01 and 3.04 Å. The E_{int} interaction energies between fragments *III* and *I* and *II* of the $[\mathbf{1}_4{-}Hal]^-$ (Table 2) decrease in the Hal sequence Cl, Br, and I, which agree with the $V_{S,min}$ values of the $[Hal]^-$ (Table 1): the more negative the $V_{S,min}$ value, the higher the corresponding E_{int}. This indicates that the strength of *ChB* and *HB*s in the $[\mathbf{1}_4{-}Hal]^-$ weakens in the Hal order Cl > Br > I. The EDD analysis[126] confirms that the formation of $[\mathbf{1}_4{-}Hal]^-$ by means of *ChB* and *HB* is accompanied by a CT as shown in Figure 5. As above, the discussed CT reflects an orbital contribution in the *ChB* in $[\mathbf{1}_4{-}Hal]^-$.

Despite growing criticism,[127–130] the QTAIM[131] topological descriptors are useful in the context of SBIs, obviously in combination with other specifiers. With QTAIM, SBIs in $[\mathbf{1}_4{-}Hal]^-$ are characterized through the properties of bond/line[128] critical points (bcp's) between interacting atoms (Figure 5), such as electron density, energy density, and Laplacian density values of the bcp's (Table 3). In general, the larger the electron density at the bcp's the stronger the interaction. If $H(r) > 0$, it means that the interaction is controlled by electrostatics, while if $H(r) < 0$, it means that the interaction is controlled by covalent forces. For *ChB*s in the $[\mathbf{1}_4{-}Hal]^-$, eight bcp's are recognized (Figure 5). The bcp's for Se…Hal, Se…N *ChB* and Hal…H *HB* are characterized by $\nabla^2\rho(r) > 0$ and $H(r) > 0$ indicating that the *ChB* and *HB* are controlled by electrostatic interactions (Table 3).[131,132]

The EDA[133] dividing the E_{int} of $[\mathbf{1}_4{-}Hal]^-$ into electrostatic, exchange, dispersion and induction (*i.e.*, orbital) contributions E_{ele}, E_{exc}, E_{dis}, and E_{ind}, respectively, was performed with symmetry-adapted perturbation theory (SAPT)[134,135] commonly used to disclose the inherent nature of intermolecular SBIs.[136–138] The EDA revealed that $E_{ele} > E_{ind} > E_{dis}$ (Table S7; SI). This indicates that the *ChB* and *HB* are mainly dominated by electrostatic interactions, with inductive (*i.e.*, orbital) and dispersion energies playing a secondary role. For $[\mathbf{1}_4{-}Hal]^-$, the contribution of E_{dis} in E_{int} is 10.6, 12.8, and 11.7% for Hal = Cl, Br, and I, respectively (Table S7).

Conclusions

In contrast to its 4,7-dicyano isomer **2**, 5,6-dicyano-2,1,3-benzoselenadiazole **1** forms isolable complexes with $[Hal]^-$ (Hal = Cl, Br, and I). Crystalline salts $[Et_4N]^+[\mathbf{1}_4{-}Hal]^-$ feature unprecedented 4:1 stoichiometry of the anions. The latter are caused by the cooperative interplay of *ChB* and *HB*. Each $[Hal]^-$ features two σ-hole-driven and two π-hole-driven *ChB*s, together with two in-plane *HB*s. Overall, each $[Hal]^-$ is six-coordinated, and the crystal structures of $[Et_4N]^+[\mathbf{1}_4{-}Hal]^-$ display a network of SBIs wherein individual $[\mathbf{1}_4{-}Hal]^-$ cannot be identified. Besides dominating electrostatic contribution, *ChB* contains a CT contribution associated with orbital interactions; dispersion interaction plays only a secondary role at the level of ~10% of the total interaction energy.

The structural situation in the solutions is not entirely clear. Very tentatively, the $\mathbf{1} + [Hal]^- \leftrightarrow [\mathbf{1}{-}Hal]^-$ equilibrium shifted towards **1** can be assumed for the reaction mixtures, with the formation/synthesis of $[\mathbf{1}_4{-}Hal]^-$ occurring during the crystallization of the $[Et_4N]^+[\mathbf{1}_4{-}Hal]^-$ employing *HB*. Further research prospects here can be associated with using charge-displacement analysis for theoretical prediction of association constants of *ChB*-bonded complexes in solution.[105] In any way, MeCN solutions of **1** display optical response on $[Hal]^-$ in the form of CT band in UV-Vis spectra featuring progressive bathochromic shift in the $[Cl]^-$, $[Br]^-$ and $[I]^-$ series, which allows identification of the individual $[Hal]^-$. Overall, **1** can be considered as a chromogenic receptor and prototype sensor of $[Hal]^-$; and the formation of $[\mathbf{1}_4{-}Hal]^-$, as anion recognition-driven template self-assembly during crystallization of $[Et_4N]^+[\mathbf{1}_4{-}Hal]^-$.

The findings of this work are useful for crystal engineering and supramolecular chemistry, the latter embracing optically-controlled anion recognition and sensing with 1,2,5- chalcogenadiazoles. Amongst those, namely Se derivatives are the most promising for anion recognition and sensing since much better studied S congeners are worse donors of *ChB*, whilst Te ones are poorly soluble and moisture sensitive. For applications, anion recognition and sensing in water are especially important. To this end, water-stable 2,1,3-benzoselenadiazoles[139] can be tailored by means of carbocyclic substitution with hydrophilic groups, e.g. $-[SO_3]^-$,[140,141] or/and by annulation with hydrophilic scaffolds. In the context of crystal engineering, this work

Table 3. The QTAIM topological descriptors of bcp's in $[\mathbf{1}_4{-}Hal]^-$ from B3LYP/def2-tzpv calculations.

Hal	bcp	1	2	3	4	5	6	7	8
Cl	$\rho(r)$	0.0237	0.0045	0.0237	0.0045	0.0114	0.0158	0.0157	0.0014
	H(r)	0.0005	0.0006	0.0005	0.0006	0.0013	0.0013	0.0013	0.0013
	$\nabla^2\rho(r)$	0.0597	0.0117	0.0597	0.0117	0.0348	0.0482	0.0482	0.0348
Br	$\rho(r)$	0.0206	0.0059	0.0205	0.0059	0.0099	0.0154	0.0153	0.0099
	H(r)	0.0002	0.0006	0.0002	0.0006	0.0013	0.0013	0.0013	0.0013
	$\nabla^2\rho(r)$	0.0454	0.0144	0.0453	0.0144	0.0307	0.0468	0.0468	0.0307
I	$\rho(r)$	0.0178	0.0040	0.0175	0.0040	0.0141	0.0127	0.0130	0.0138
	H(r)	0.0001	0.0004	0.0001	0.0004	0.0013	0.0014	0.0014	0.0013
	$\nabla^2\rho(r)$	0.0323	0.0094	0.0321	0.0093	0.0416	0.0402	0.0409	0.0409

demonstrates how minor variations of the molecular structure allow to tune the propensity of chalcogenadiazole derivatives towards cocrystallization with Lewis bases, while the magnitude of $V_{S,max}$ of the σ-hole at a chalcogen remains almost the same, unlike in previous reports, where the main reason of the cocrystallization is a certain magnitude of $V_{S,Max}$ at the σ-hole at a chalcogen. This is achieved by placing an additional SBI site (*HB* donor moiety) into the molecule so that both sites can interact cooperatively with the same Lewis basic site ($[Hal]^-$ in our case), providing the synergistic effect. This approach may be further developed as a crystal engineering tool.

Experimental and Computational Section

General

Compounds **1**,[142] **2**,[143] and **3**[144] were synthesized according to the literature procedures and their single crystals were suitable for XRD. Salts $[Et_4N]^+[Hal]^-$ and $[Bu_4N]^+[Hal]^-$ (Hal = Cl, Br, I) were obtained from J&K Scientific and used without purification. MeCN was dried with P_2O_5 and distilled over CaH_2; Et_2O was distilled over sodium wire/benzophenone.

Solution UV-Vis spectra, including spectrophotometric titration, were collected in MeCN with SF-2000 spectrophotometer. Solid-state Vis spectra were obtained as Kubelka-Munk function[107] of the diffuse reflectance spectra measured on a Shimadzu UV-3101 instrument for mixtures of **1** or $[Et_4N]^+[\mathbf{1}_4{-}Hal]^-$ with $BaSO_4$ (~5 wt.%). FL spectra were collected with Varian Cary Eclipse fluorescence spectrophotometer.

The ^1H, ^{13}C, ^{35}Cl, and ^{77}Se NMR spectra were measured in MeCN at 600, 151, 59, and 114 MHz, respectively, with a Bruker AV-600 machine using Me_4Si (TMS), aqueous $[K]^+[Cl]^-$, and Me_2Se as standards.

ESI-MS spectra were taken with a Bruker Daltonik micrOTOF-Q hybrid quadrupole time-of-flight mass spectrometer equipped with electrospray ionization sources for solutions of **1** in MeCN saturated with $[Et_4N]^+[Hal]^-$.

Elemental analyses (EA) were performed for C, H and N with a CHNS-Analyzer Euro EA 300; for Cl, Br, and I, with mercurimetric titration of halides in the combustion products using diphenylcarbazone as an indicator; and for Se, with microwave plasma atomic emission spectroscopy (MP-AES) using Agilent 4100 MP-AES instrument and samples prepared by Schöniger method.

Syntheses

Polycrystalline samples: Stirred solutions of 0.04 mmol of $[Et_4N]^+[Hal]^-$ and 40 mg (0.17 mmol) of **1** in 4 ml of MeCN were heated to boiling, rapidly concentrated to 1 ml under the stream of compressed air, and cooled to −20 °C. The precipitates were filtered off and dried on air.

Complex $[Et_4N]^+[\mathbf{1}_4{-}Cl]^-$ was obtained in the form of yellow powder, 24 mg (51%). EA, found/calculated for $C_{40}H_{28}ClN_{17}Se_4$, %: C 43.59/43.75, H 2.21/H 2.57, Cl 3.57/3.23, N 21.58/21.68, Se 28.37/28.77. UV-Vis (MeCN), λ_{max}, nm: ~385 (SI).

Complex $[Et_4N]^+[\mathbf{1}_4{-}Br]^-$ was obtained in the form of orange powder, 28 mg (57%). EA, found/calculated for $C_{40}H_{28}BrN_{17}Se_4$, %: C 41.70/42.05, H 2.29/2.47, Br 7.29/6.99, N 20.58/20.84, Se 27.99/27.65. UV-Vis (MeCN), λ_{max}, nm: ~400 (SI).

Complex $[Et_4N]^+[\mathbf{1}_4{-}I]^-$ was obtained in the form of red powder, 33 mg (65%). EA, found/calculated for $C_{40}H_{28}IN_{17}Se_4$, %: C 39.97/40.39, H 2.25/2.37, I 10.85/10.67, N 19.74/20.02, Se 26.00/26.55. UV-Vis (MeCN), λ_{max}, nm: 461 (SI).

Attempts of fast precipitation of the complexes from the MeCN solutions with 4 ml of diethyl ether yielded only starting materials.

Single crystals: Solutions of **1** (9 mg, 0.04 mmol) and 0.04, 0.08, or 0.12 mmol of $[Et_4N]^+[Hal]^-$ in 2 ml of MeCN underwent slow evaporation in air (1-2 weeks). The solid residues were mixtures of the starting materials with crystals of $[Et_4N]^+[\mathbf{1}_4{-}Hal]^-$ complexes. The mixtures were separated mechanically. The $[Et_4N]^+[\mathbf{1}_4{-}Br]^-$ and $[Et_4N]^+[\mathbf{1}_4{-}I]^-$ were obtained in the form of orange needles and red plates, respectively, suitable for XRD. The $[Et_4N]^+[\mathbf{1}_4{-}Cl]^-$ was obtained in the form of yellow crystals unsuitable for XRD. In the form of yellow needles suitable for XRD, $[Et_4N]^+[Cl]^-$ was prepared by ambient-temperature diffusion of pentane vapors into an equimolar solution of the starting materials in CH_2Cl_2.

X-ray crystallography

The XRD experiments (Figures 3 and 4; SI) were performed with a Bruker Kappa Apex II CCD diffractometer by using a graphite-monochromated MoKα irradiation. The structures were solved by the direct method using the *SHELX-97*[145] program and refined by full-matrix least-squares method against all F^2 in anisotropic approximation using the *OLEX2* program.[146] The H atoms positions were calculated with the riding model. Absorption corrections were applied using the empirical multiscan method with the *SADABS* programs.[147] The obtained crystal structures were analyzed for shortened contacts between non-bonded atoms using the *PLATON*[148] and *MERCURY*[149] programs.

Deposition Numbers 2241710 (for **1**), 2241711 (for $[Et_4N]^+[\mathbf{1}_4{-}Br]^-$), 2241712 (for $[Et_4N]^+[\mathbf{1}_4{-}I]^-$), 2266273 (for **3**) and 2266274 (for $[Et_4N]^+[\mathbf{1}_4{-}Cl]^-$) contain the supplementary crystallographic data for this paper. These data are provided free of charge by the joint Cambridge Crystallographic Data Centre and Fachinformationszentrum Karlsruhe Access Structures service.

Quantum chemical calculations

The geometric configurations of $[\mathbf{1}_n{-}Hal]^-$ (n = 2, 4) were optimized at the B3LYP/def2-tzvp level of theory with ECP for I, and frequency calculations were performed to confirm that the optimized geometries have no imaginary frequencies. The QTAIM[131] topological analysis of bcp's[128] was conducted on the B3LYP/def2-tzvp. The EDA was performed by means of SAPT[134,135] using the PSI4 method[150] with the def2-tzvpp basis set on the SAPT0 level. The E_{int} interaction energy in the $[\mathbf{1}_n{-}Hal]^-$ (n = 2, 4) was calculated as $E_{int} = E_{comp} - nE_1 + E_{bsse}$, where E_{comp} is the energy of the optimized $\mathbf{1}_n{-}Hal]^-$, E_1 is the energy of molecule **1**, *n* is the number of molecules **1**, and E_{bsse} is the basis set superposition error assessed by the Boys and Bernardy counterpoise method.[151] For the DFT calculations and MEP, QTAIM, EDA, and EDD analyses, the *Gaussian09*,[152] *Multiwfn*,[153] and *VMD*[154] software were employed.

TD-DFT[108,109] calculations of UV-Vis spectra of the $[\mathbf{1}{-}Hal]^-$ and $[\mathbf{1}_4{-}Hal]^-$ were performed for the B97-D3/def2-tzvp[155–158]-optimized geometries at the B2PLYP/def2-tzvp level of theory[110] for gas phase and solution applying the C-PCM[112,159] for MeCN solvent; for I, ECP was used. The Becke-Johnson damping function and the Grimme geometrical counterpoise (gCP) correction scheme were used in all calculations.[156,160,161] The calculations were performed by using *the ORCA 4.2.0* suite of programs.[162,163]

Supporting Information

The Supporting information for this article contains XRD, solution and solid-state UV-Vis, variable-temperature ^{35}Cl and ^{77}Se NMR, DFT, TD-DFT, QTAIM, EDD and EDA data. Within the Supporting Information, the authors have cited additional references (Ref. [164–169]).

Acknowledgements

The authors are grateful to Dr. Elena A. Pritchina and Dr. Vera D. Tikhova for valuable discussions and to Dr. Elena V. Karpova and Irina V. Yushina for FL and solid-state UV-Vis measurements, respectively, as well as Dr. Andrey A. Nefedov for ESI-MS measurements. The Novosibirsk authors are grateful to the Russian Science Foundation (project no. 21-73-10291; synthesis, XRD, NMR, UV-Vis spectroscopy, MEP and TD-DFT calculations) and the Ministry for Science and Higher Education of Russian Federation (the State Assignment, project no. 122040400035-3; ESI-MS and FL spectroscopy) for financial support; and to Prof. Nina P. Gritsan and her group for computational resources, and to the Multi-Access Chemical Research Center and Collective Usage Center, Siberian Branch of the Russian Academy of Sciences, for instrumental facilities. The Chengdu authors are grateful to the Fundamental Research Funds for the Central Universities (project no. 2682023GF027; gas-phase DFT calculations, QTAIM, EDD and EDA analyses) for financial support.

Conflict of Interests

The authors declare no conflict of interest.

Data Availability Statement

The data that support the findings of this study are available in the supplementary material of this article.

Keywords: chalcogen bonding · chalcogenadiazoles · cooperativity · hydrogen bonding · noncovalent interactions

[1] N. W. Alcock, *Adv. Inorg. Chem. Radiochem.* **1972**, *15*, 1–58.
[2] C. B. Aakeröy, S. Alavi, L. Brammer, D. L. Bryce, T. Clark, J. L. Del Bene, A. J. Edwards, C. Esterhuysen, T. N. Guru Row, P. Kennepohl, A. C. Legon, G. O. Lloyd, J. S. Murray, W. T. Pennington, P. Politzer, K. E. Riley, S. V. Rosokha, S. Scheiner, S. Tsuzuki, I. Vargas-Baca, *Faraday Discuss.* **2017**, *203*, 131–163.
[3] B. Silvi, E. Alikhani, H. Ratajczak, *J. Mol. Model.* **2020**, *26*, 62.
[4] P. Molina, F. Zapata, A. Caballero, *Chem. Rev.* **2017**, *117*, 9907–9972.
[5] *Comprehensive Supramolecular Chemistry II,* Ed. J. L. Atwood, Vol. 3 (*Supramolecular Receptors*), Elsevier, **2017**.
[6] G. W. Gokel, W. M. Leevy, M. E. Weber, *Chem. Rev.* **2004**, *104*, 2723–2750.
[7] P. D. Beer, P. A. Gale, *Angew. Chem. Int. Ed.* **2001**, *40*, 486–516.
[8] V. B. Shur, I. A. Tikhova, *Russ. Chem. Bull.* **2003**, *52*, 2539–2554.
[9] M. R. Haneline, R. E. Taylor, F. P. Gabbai, *Chem. Eur. J.* **2003**, *9*, 5188–5193.
[10] *Anion Receptor Chemistry*, Eds. J. L. Sessler, P. A. Gale, W.-S. Cho, RSC Publishing, **2006**.
[11] P. A. Gale, *Chem. Commun.* **2011**, 82–86.
[12] N. A. Itsikson, Yu. Yu. Morzherin, A. I. Matern, O. N. Chupakhin, *Russ. Chem. Rev.* **2008**, *77*, 751–764.
[13] J. T. Davis, P. A. Gale, R. Quesado, *Chem. Soc. Rev.* **2020**, *49*, 6059–6086.
[14] G. R. Desiraju, *J. Am. Chem. Soc.* **2013**, *135*, 9952–9967.
[15] A. K. Nangia, G. R. Desiraju, *Angew. Chem. Int. Ed.* **2019**, *58*, 4100–4107.
[16] J. S. Murray, G. Resnati, P. Politzer, *Faraday Discuss.* **2017**, *203*, 113–130.
[17] N. Busschaert, C. Caltagirone, W. Van Rossom, P. A. Gale, *Chem. Rev.* **2015**, *115*, 8083–8155.
[18] P. A. Gale, C. Caltagirone, *Chem. Soc. Rev.* **2015**, *44*, 4212–4227.
[19] M. Mansha, S. A. Khan, M. A. Aziz, A. Z. Khan, S. Ali, M. Khan, *Chem. Rec.* **2022**, *22*, e202200059.
[20] A. Pal, M. Karmakar, S. P. Bhatta, A. Thakur, *Coord. Chem. Rev.* **2021**, *448*, 214167.
[21] E. Arunan, G. R. Desiraju, R. A. Klein, J. Sadlej, S. Scheiner, I. Alkorta, D. C. Clary, R. H. Crabtree, J. J. Dannenberg, P. Hobza, H. Kjaergaard, A. C. Legon, B. Mennucci, D. J. Nesbitt, *Pure Appl. Chem.* **2011**, *83*, 1637–1641.
[22] S. J. Grabowski, *Understanding Hydrogen Bonds: Theoretical and Experimental Views*, RSC, **2020**.
[23] S. J. Grabowski, *Phys. Chem. Chem. Phys.* **2017**, *19*, 29742–29759.
[24] G. Cavallo, P. Metrangolo, R. Milani, T. Pilati, A. Priimagi, G. Resnati, G. Terraneo, *Chem. Rev.* **2016**, *116*, 2478–2601.
[25] G. Desiraju, P. S. Ho, L. Kloo, A. C. Legon, R. Marquardt, P. Metrangolo, P. Politzer, G. Resnati, *Pure Appl. Chem.* **2013**, *85*, 1711–1713.
[26] R. Hein, P. D. Beer, *Chem. Sci.* **2022**, *13*, 7098–7125.
[27] M. H. Kolář, P. Hobza, *Chem. Rev.* **2016**, *116*, 5155–5187.
[28] H. Wang, W. Wang, W. J. Jin, *Chem. Rev.* **2016**, *116*, 5072–5104.
[29] M. S. Taylor, *Coord. Chem. Rev.* **2020**, *413*, 213270.
[30] T. Bunchuay, A. Docker, U. Eiamprasert, P. Surawatanawong, A. Brown, P. D. Beer, *Angew. Chem. Int. Ed.* **2020**, *59*, 12007–12012.
[31] A. D. Docker, C. H. Guthrie, H. Kuhn, P. D. Beer, *Angew. Chem. Int. Ed.* **2021**, *60*, 21973–21978.
[32] C. B. Aakeroy, D. L. Bryce, G. R. Desiraju, A. Frontera, A. C. Legon, F. Nicotra, K. Rissanen, S. Scheiner, G. Terraneo, P. Metrangolo, G. Resnati, *Pure Appl. Chem.* **2019**, ***91***, 1889–1892.
[33] S. Kolb, G. A. Oliver, B. Werz, in *Comprehensive Inorganic Chemistry III*, Elsevier, **2023**, 602–651.
[34] L. Vogel, P. Wonner, S. M. Huber, *Angew. Chem. Int. Ed.* **2019**, *58*, 1880–1891.
[35] V. Angarov, S. Kozuch, *New J. Chem.* **2018**, *42*, 1413–1422.
[36] E. V. Bartashevich, Yu. V. Matveychuk, S. E. Mikhitdinova, S. A. Sobolev, M. G. Khrenova, V. G. Tsirelson, *Theor. Chem. Acc.* **2020**, *139*, 26.
[37] D. Romito, P. C. Ho, I. Vargas-Baca, D. Bonifazi, in: *Chalcogen Chemistry: Fundamentals and Applications*, RSC Publishing, **2023**, pp. 494–528.
[38] M. C. Aragoni, Yu. Torubaev, in: *Chalcogen Chemistry: Fundamentals and Applications*, RSC Publishing, **2023**, pp. 435–475.
[39] P. Scilabra, G. Terraneo, G. Resnati, *Acc. Chem. Res.* **2019**, *52*, 1313–1324.
[40] P. Pale, V. Mamane, *ChemPhysChem* **2023**, *24*, e202200481.
[41] K. T. Makhmudov, M. N. Kopylovich, M. F. C. Guerdes da Silva, A. J. L. Pombeiro, *Dalton Trans.* **2017**, *46*, 10121–10138.
[42] S. Scheiner, *Chem. Eur. J.* **2016**, *22*, 18850–18858.
[43] G. E. Garrett, G. L. Gibson, R. N. Strauss, D. S. Seferos, M. S. Taylor, *J. Am. Chem. Soc.* **2015**, *137*, 4126–4133.
[44] G. E. Garrett, E. I. Carrera, D. S. Seferos, M. S. Taylor, *Chem. Commun.* **2016**, *52*, 9881–9884.
[45] P. C. Ho, J. Z. Wang, F. Meloni, I. Vargas-Baca, *Coord. Chem. Rev.* **2020**, *422*, 213464.
[46] N. Biot, D. Bonifazi, *Coord. Chem. Rev.* **2020**, *413*, 213243.
[47] E. Navarro-García, B. Galmés, M. D. Velasco, A. Frontera, A. Caballero, *Chem. Eur. J.* **2020**, *26*, 4706–4713.
[48] S. Schneider, *Crystals* **2023**, *13*, 766.
[49] S. Scheiner, J. Lu, *Chem. Eur. J.* **2018**, *24*, 8167–8177.
[50] G. Cavallo, P. Metrangolo, T. Pilati, G. Resnati, G. Terraneo, *Cryst. Growth Des.* **2016**, *14*, 2697–2702.
[51] S. Scheiner, *J. Phys. Chem. A* **2022**, *126*, 1194–1203.
[52] R. Pollice, P. Chen, *Angew. Chem. Int. Ed.* **2019**, *58*, 9758–9769.
[53] J. P. Wagner, P. R. Schneider, *Angew. Chem. Int. Ed.* **2015**, *54*, 12274–12296.
[54] D. J. Pascoe, K. B. Ling, S. L. Cockroft, *J. Am. Chem. Soc.* **2017**, *189*, 15160–15167.
[55] J. S. Murray, P. Politzer, *WIREs Comput. Mol. Sci.* **2011**, *1*, 153–163.

[56] J. S. Murray, P. Politzer, *WIREs Comput. Mol. Sci.* **2017**, *7*, e1326.
[57] C. H. Suresh, G. S. Remya, P. K. Anjalikrishna, *WIREs Comput. Mol. Sci.* **2022**, *12*, e1601.
[58] B. Mallada, A. Gallarado, M. Lananec, B. de la Torre, V. Špirko, P. Hobza, J. Jelinek, *Science* **2021**, *374*, 863–867.
[59] P. Politzer, J. S. Murray, *Crystals* **2019**, *9*, 165.
[60] S. Schneider, *J. Phys. Chem. A* **2021**, *125*, 6514–6521.
[61] S. Schneider, *ChemPhysChem* **2023**, *24*, e202200936.
[62] E. A. Katlenok, M. L. Kuznetsov, N. A. Semenov, N. A. Bokach, V. Yu. Kukushkin, *Inorg. Chem. Front.* **2023**, *10*, 3065–3081.
[63] J. S. Murray, P. Lane, T. Clark, K. E. Riley, P. Politzer, *J. Mol. Model.* **2012**, *18*, 541–548.
[64] J. S. Murray, P. Lane, T. Clark, P. Politzer, *J. Mol. Model.* **2007**, *13*, 1033–1038.
[65] S. Kozuch, *Phys. Chem. Chem. Phys.* **2016**, *18*, 30366–30369.
[66] A. Bauzá, T. J. Mooibroek, A. Frontera, *ChemPhysChem* **2015**, *16*, 2496–2517.
[67] I. V. Alabugin, K. M. Gilmore, P. W. Peterson, *WIREs Comput. Mol. Sci.* **2011**, *1*, 109–141.
[68] P. Schwerdtfeger, J. K. Nagle, *Mol. Phys.* **2019**, *117*, 1200–1225.
[69] J. Y. C. Lim, J. Y. Liew, P. D. Beer, *Chem. Eur. J.* **2018**, *24*, 14560–14566.
[70] V. Jurásková, F. Célerse, R. Laplaza, C. Corminboeuf, *J. Chem. Phys.* **2022**, *156*, 154112.
[71] R. Hein, A. Docker, J. J. Davis, P. D. Beer, *J. Am. Chem. Soc.* **2022**, *144*, 8827–8836.
[72] E. A. Radiush, E. A. Pritchina, E. A. Chulanova, A. A. Dmitriev, I. Yu. Bagryanskaya, A. M. Z. Slawin, J. D. Woollins, N. P. Gritsan, A. V. Zibarev, N. A. Semenov, *New J. Chem.* **2022**, *46*, 14490–14501.
[73] N. A. Semenov, A. V. Lonchakov, N. A. Pushkarevsky, E. A. Suturina, V. V. Korolev, E. Lork, V. G. Vasiliev, S. N. Konchenko, J. Beckmann, N. P. Gritsan, A. V. Zibarev, *Organometallics* **2014**, *33*, 4302–4314.
[74] N. A. Semenov, D. E. Gorbunov, M. V. Shakhova, G. E. Salnikov, I. Yu. Bagryanskaya, V. V. Korolev, J. Beckmann, N. P. Gritsan, A. V. Zibarev, *Chem. Eur. J.* **2018**, *24*, 12983–12991.
[75] E. A. Chulanova, E. A. Radiush, I. K. Shundrina, I. Yu. Bagryanskaya, N. A. Semenov, J. Beckmann, N. P. Gritsan, A. V. Zibarev, *Cryst. Growth Des.* **2020**, *20*, 5868–5879.
[76] N. A. Pushkarevsky, E. A. Chulanova, L. A. Shundrin, A. I. Smolentsev, G. E. Salnikov, E. A. Pritchina, A. M. Genaev, I. G. Irtegova, I. Yu. Bagryanskaya, S. N. Konchenko, N. P. Gritsan, J. Beckmann, A. V. Zibarev, *Chem. Eur. J.* **2019**, *25*, 806–816.
[77] N. A. Semenov, A. V. Lonchakov, N. P. Gritsan, A. V. Zibarev, *Russ. Chem. Bull.* **2015**, *64*, 499–510.
[78] N. A. Semenov, N. A. Pushkarevsky, J. Beckmann, P. Finke, E. Lork, R. Mews, I. Yu. Bagryanskaya, Yu. V. Gatilov, S. N. Konchenko, V. G. Vasiliev, A. V. Zibarev, *Eur. J. Inorg. Chem.* **2012**, *2012*, 3693–3703.
[79] E. A. Suturina, N. A. Semenov, A. V. Lonchakov, I. Yu. Bagryanskaya, Yu. V. Gatilov, I. G. Irtegova, N. V. Vasilieva, E. Lork, R. Mews, N. P. Gritsan, A. V. Zibarev, *J. Phys. Chem. A* **2011**, *115*, 4851–4860.
[80] V. Kumar, Y. Xu, D. L. Bryce, *Chem. Eur. J.* **2020**, *26*, 3275–3286.
[81] T. Nang, J. S. Ovens, D. L. Bryce, *Acta Crystallogr. Sect. C* **2022**, *78*, 517–523.
[82] 1,2,5-Chalcogenadiazoles reveal Lewis ambiphilicity and form N-bonded complexes with Lewis acids, e.g. BR_3, as well; when R = Hal, the complexes reveal intramolecular *ChB*: J. Lee, L. M. Lee, Z. Arnott, H. Jenkins, J. F. Britten, I. Vargas-Baca, *New J. Chem.* **2018**, *42*, 10555–10562.
[83] L. Zhang, Y. Zheng, X. Li, X. Zheng, *J. Mol. Model.* **2022**, *28*, 248.
[84] Y. Xu, V. Kumar, M. J. Z. Bradshaw, D. L. Bryce, *Cryst. Growth Des.* **2020**, *20*, 7910–7920.
[85] L. Chen, J. Xiang, Y. Zhao, Q. Yan, *J. Am. Chem. Soc.* **2018**, *140*, 7079–7080.
[86] L. S. Konstantinova, E. A. Knyazeva, Yu. V. Gatilov, S. G. Zlotin, O. A. Rakitin, *Russ. Chem. Bull.* **2018**, *67*, 95–101.
[87] T. Shimajiri, H.-P. Jaquot de Rouville, V. Heltz, A. Akutagawa, T. Fukushima, I. Ishikagi, T. Suzuki, *SynLett* **2023**, *34*, 1978–1990 .
[88] A. V. Zibarev, R. Mews, in: *Selenium and Tellurium Chemistry: From Small Molecules to Biomolecules and Materials*, Eds. J. D. Woollins and R. S. Laitinen, Springer, **2011**, pp. 123–149.
[89] B. Li, X. Wang, H. Wang, Q. Song, Y. Ni, H. Wang, X. Wang, *J. Mol. Struct.* **2022**, *1265*, 133371.
[90] For bidentate Lewis bases bifurcated ChBs based on one σ-hole are discussed: S. Mehrparvar, C. Wölper, R. Gleiter, G. Haberhauser, *Org. Mater.* **2022**, *4*, 43–52.
[91] J. Alfuth, B. Zadykowicz, A. Sikorski, T. Polonsky, K. Eichstaed, T. Olszewska, *Materials* **2020**, *13*, 4908.
[92] S. Scheiner, M. Michalczyk, W. Zierkiewicz, *Coord. Chem. Rev.* **2020**, *405*, 213136.
[93] N. A. Semenov, *Ph. D. Dissertation*, Novosibirsk, **2013** (in Russian) .
[94] M. L. Lee, V. B. Corless, M. Tran, H. Jenkins, J. F. Britten, I. Vargas-Baca, *Dalton Trans.* **2016**, *45*, 3285–3293.
[95] M. Risto, R. W. Reed, C. M. Robertson, R. Oilunkaniemi, R. S. Laitinen, R. T. Oakley, *Chem. Commun.* **2008**, 3278–3280.
[96] J. L. Dutton, P. J. Ragogna, *Inorg. Chem.* **2009**, *48*, 1722–1730.
[97] The $[F]^-$ is not involved in this study to be used in another research on fluoride-ion affinity (FIA) of a broad set of 1,2,5-chalcogenadiazoles as a quantitative descriptor of their Lewis acidity. Nowadays, FIA is considered as valuable quantitative descriptor of Lewis acidity.
[98] P. Erdmann, J. Leitner, J. Schwarz, L. Greb, *ChemPhysChem* **2020**, *21*, 987–994.
[99] P. Erdmann, L. Greb, *ChemPhysChem* **2021**, *22*, 935–943.
[100] P. Erdmann, L. Greb, *Angew. Chem. Int. Ed.* **2022**, *61*, e202114550.
[101] E. A. Chulanova, E. A. Radiush, N. A. Semenov, E. Hupf, I. G. Irtegova, Yu. S. Kosenkova, I. Yu. Bagryanskaya, L. A. Shundrin, J. Beckmann, A. V. Zibarev, *ChemPhysChem* **2023**, *24*, e202200876.
[102] K. Eichstaed, A. Wasilewska, B. Wicher, M. Gdaniec, T. Polonski, *Cryst. Growth Des.* **2016**, *16*, 1282–1293.
[103] X. Zhang, Q. Li, J. B. Ingels, A. C. Simmonett, S. E. Wheeler, X. Xie, R. B. King, H. F. Schaefer, F. A. Cotton, *Chem. Commun.* **2006**, *7*, 758–760.
[104] E. Parman, M. Lõkov, J. Järviste, S. Tshepelevitsh, N. A. Semenov, E. A. Chulanova, G. E. Salnikov, D. O. Prima, Yu. G. Slizhov, I. Leito, A. V. Zibarev, *ChemPhysChem* **2021**, *22*, 2329–2335.
[105] G. Ciancaleoni, C. Santi, M. Ragni, A. L. Braga, *Dalton Trans.* **2015**, *44*, 20168–20175.
[106] F. De Vleeschouwer, M. Denayer, B. Pinter, P. Geerling, F. De Proft, *J. Comput. Chem.* **2018**, *39*, 557–572.
[107] R. Alcaraz de la Osa, I. Iparragirre, D. Ortiz, J. M. Saiz, *ChemTexts* **2020**, *6*, 2.
[108] *Time-Dependent Density Functional Theory*, Eds. M. A. L. Marques, C. A. Ullrich, F. Nogueira, A. Rubio, K. Burke, E. K. U. Gross, Springer, **2006**.
[109] A. Dreuw, M. Head-Gordon, *Chem. Rev.* **2005**, *105*, 4009–4037.
[110] S. Grimme, F. Neese, *J. Chem. Phys.* **2007**, *127*, 154116.
[111] E. A. Chulanova, E. A. Radiush, Y. Balmohammadi, J. Beckmann, S. Grabowsky, A. V. Zibarev, *CrystEngComm* **2023**, *25*, 391–402.
[112] M. Cossi, N. Rega, G. Scalamani, V. Barone, *J. Comput. Chem.* **2003**, *24*, 669–681.
[113] A. C. Gomes, G. Biswas, A. Banerjee, W. L. Duax, *Acta Crystallogr. Sect. C* **1989**, *45*, 73–75.
[114] Previously, XRD structure of compound **3** was published without thermal parameters (CCDC 1109027); in this work, it is reinvestigated (CCDC 2266273; SI).
[115] S. Kawaguchi, T. Shimariji, T. Akutagawa, T. Fukushima, Y. Ishigaki, T. Suzuki, *Bull. Chem. Soc. Jpn* **2023**, *96*, 631–635.
[116] A. F. Cozzolino, I. Vargas-Baca, S. Mansour, A. H. Mahmoudkhani, *J. Am. Chem. Soc.* **2005**, *127*, 3184–3190.
[117] A. F. Cozzolino, I. Vargas-Baca, *J. Organomet. Chem.* **2007**, *692*, 2654–2657.
[118] E. R. T. Tiekink, *CrystEngComm* **2023**, *25*, 9–39.
[119] A. Pomogaeva, F. L. Gu, A. Imamura, Y. Aoki, *Theor. Chem. Acc.* **2010**, *125*, 453–460.
[120] N. A. Semenov, E. A. Radiush, E. A. Chulanova, A. M. Z. Slawin, J. D. Woollins, E. M. Kadilenko, I. Yu. Bagryanskaya, I. G. Irtegova, A. S. Bogomyakov, L. A. Shundrin, N. P. Gritsan, A. V. Zibarev, *New J. Chem.* **2019**, *43*, 16331–16337.
[121] M. Mantina, A. C. Chamberlin, R. Valero, C. J. Cramer, D. G. Truhlar, *J. Phys. Chem. A* **2009**, *113*, 5806–5812.
[122] R. S. Rowland, R. Taylor, *J. Phys. Chem.* **1996**, *100*, 7384–7391.
[123] S. Scheiner, *Phys. Chem. Chem. Phys.* **2022**, *24*, 28944–28955.
[124] S. Goswami, A. Hazra, M. Kumar Das, *Tetrahedron Lett.* **2010**, *51*, 3320–3323.
[125] Y. Ishigaki, K. Shimomura, K. Asai, T. Shimajiri, T. Akutawaga, T. Fukushima, T. Suzuki, *Bull. Chem. Soc. Jpn.* **2022**, *95*, 522–531.
[126] E. Pastorczak, C. Corminboeuf, *J. Chem. Phys.* **2017**, *146*, 120901.
[127] S. Shahbazian, *Int. J. Quantum Chem.* **2018**, *118*, e25637.
[128] S. Shahbazian, *Chem. Eur. J.* **2018**, *24*, 5401–5405.
[129] M. Jabloński, *ChemistryOpen* **2019**, *8*, 497–507.
[130] R. Taylor, *CrystEngComm* **2020**, *22*, 7145–7151.
[131] R. W. F. Bader, *Atoms in Molecules: A Quantum Theory*, Cambridge University Press, **1991**.

[132] E. Espinosa, I. Alkorta, J. Elguero, E. Molins, *J. Chem. Phys.* **2002**, *117*, 5529–5542.
[133] There are many different EDA schemes; for discussion, see e.g.: L. Zhao, M. von Hopffgarten, M. D. Andrada, G. Frenking, *WIREs Comput. Mol. Sci.* **2018**, *8*, e1345.
[134] G. Jansen, *WIREs Comput. Mol. Sci.* **2014**, *4*, 127–144.
[135] K. Patkowski, *WIREs Comput. Mol. Sci.* **2020**, *10*, e1452.
[136] D. Zhou, G. Li, K. B. Moore, Y. Xie, K. A. Petersen, H. F. Schaefer, *J. Chem. Theory Comput.* **2018**, *14*, 5118–5127.
[137] Z. Liu, T. Lu, Q. Chen, *Carbon* **2021**, *171*, 514–523.
[138] S. Emamian, T. Lu, H. Kruse, H. Emamian, *J. Comput. Chem.* **2019**, *40*, 2868–2881.
[139] T. Chivers, R. S. Laitinen, *Chalcogen-Nitrogen Chemistry: From Fundamentals to Applications in Biological, Physical and Materials Sciences*, World Scientific, **2021**.
[140] Z. V. Todres, S. I. Zhdanov, V. Sh. Tsveniashvili, *Russ. Chem. Bull.* **1968**, *17*, 934–939.
[141] C. Toriumi, T. Santa, K. Imai, *Proc. Japan Acad. B* **2003**, *79*, 137–140.
[142] E. H. Mørkved, S. M. Neset, O. Bjørlo, H. Kjøsen, G. Hvistendahl, F. Mo, T. Bartfai, Ü Langel, *Acta Chem. Scand.* **1995**, *49*, 658–662; Langel, *Acta Chem. Scand.* **1995**, *49*, 658–662.
[143] R. Edwards, I. Cummins, P. Steel, *WO2009034396*, **2009**.
[144] R. A. Aitken, *Sci. Synth.* **2004**, *13*, 806–807.
[145] G. M. Sheldrick, *Acta Crystallogr. Sect. C* **2015**, *71*, 3–8.
[146] O. V. Dolomanov, L. J. Bourhis, R. J. Gildea, J. A. K. Howard, H. Puschmann, *J. Appl. Crystallogr.* **2009**, *42*, 339–341.
[147] *SADABS, v. 2008–1*, Bruker AXS Inc., Madison, WI, USA, *2008*.
[148] A. L. Spek, *J. Appl. Crystallogr.* **2003**, *36*, 7–13.
[149] C. F. Macrae, P. R. Edgington, P. McCabe, E. Pidcock, G. P. Shields, R. Taylor, M. Towler, J. van de Streek, *J. Appl. Crystallogr.* **2006**, *39*, 453–457.
[150] D. G. A. Smith, L. A. Burns, A. C. Simmonett, R. M. Parrish, M. C. Schieber, R. Galvelis, P. Kraus, H. Kruse, R. Di Remigio, A. Alenaizan, A. M. James, S. Lehtola, J. P. Misiewicz, M. Scheurer, R. A. Shaw, J. B. Schriber, Y. Xie, Z. L. Glick, D. A. Sirianni, J. S. O'Brien, J. M. Waldrop, A. Kumar, E. G. Hohenstein, B. P. Pritchard, B. R. Brooks, H. F. Schaefer, A. Yu. Sokolov, K. Patkowski, A. E. DePrince, U. Bozkaya, R. A. King, F. A. Evangelista, J. M. Turney, T. D. Crawford, C. D. Sherrill, *J. Chem. Phys.* **2020**, *152*, 184108.
[151] M. Gray, P. E. Bowling, J. M. Herbert, *J. Chem. Theory Comput.* **2022**, *18*, 6742–6756.
[152] M. J. Frisch, G. W. Trucks, H. B. Schlegel, G. E. Scuseria, M. A. Robb, J. R. Cheeseman, G. Scalmani, V. Barone, B. Mennucci, G. A. Petersson, H. Nakatsuji, M. Caricato, X. Li, H. P. Hratchian, A. F. Izmaylov, J. Bloino, G. Zheng, J. L. Sonnenberg, M. Hada, M. Ehara, K. Toyota, R. Fukuda, J. Hasegawa, M. Ishida, T. Nakajima, Y. Honda, O. Kitao, H. Nakai, T. Vreven, J. A. Montgomery Jr., J. E. Peralta, F. Ogliaro, M. Bearpark, J. J. Heyd, E. Brothers, K. N. Kudin, V. N. Staroverov, R. Kobayashi, J. Normand, K. Raghavachari, A. Rendell, J. C. Burant, S. S. Iyengar, J. Tomasi, M. Cossi, N. Rega, J. M. Millam, M. Klene, J. E. Knox, J. B. Cross, V. Bakken, C. Adamo, J. Jaramillo, R. Gomperts, R. E. Stratmann, O. Yazyev, A. J. Austin, R. Cammi, C. Pomelli, J. W. Ochterski, R. L. Martin, K. Morokuma, V. G. Zakrzewski, G. A. Voth, P. Salvador, J. J. Dannenberg, S. Dapprich, A. D. Daniels, Ö. Farkas, J. B. Foresman, J. V. Ortiz, J. Cioslowski, D. J. Fox, *Gaussian 09*, Gaussian, Inc., Wallingford CT, 2009.
[153] T. Lu, F. Chen, *J. Comput. Chem.* **2012**, *33*, 580–592.
[154] W. Humphrey, A. Dalke, K. Schulten, *J. Mol. Graphics* **1996**, *14*, 33–38.
[155] S. Grimme, J. Antony, S. Ehrlich, H. Krieg, *J. Chem. Phys.* **2010**, *132*, 154104.
[156] S. Grimme, *J. Comput. Chem.* **2006**, *27*, 1787–1799.
[157] F. Weigend, R. Ahlrichs, *Phys. Chem. Chem. Phys.* **2005**, *7*, 3297–3305.
[158] F. Weigend, *Phys. Chem. Chem. Phys.* **2006**, *8*, 1057–1065.
[159] V. Barone, M. Cossi, *J. Phys. Chem. A* **1998**, *102*, 1995–2001.
[160] S. Grimme, S. Ehrlich, L. Goerigk, *J. Comput. Chem.* **2011**, *32*, 1456–1465.
[161] H. Kruse, S. Grimme *J. Chem. Phys.* **2012**, *136*, 154101.
[162] F. Neese, *WIREs Comput. Mol. Sci.* **2012**, *2*, 73–78.
[163] F. Neese, F. Wennmohs, U. Becker and C. Riplinger, *J. Chem. Phys.* **2020**, *152*, 224108.
[164] L. Brammer, A. Peuronen, T. M. Roseveare, *Acta Crystallogr. Sect. C* **2023**, *79*, 204–216.
[165] V. Kumar, Y. Xu, C. Leroy, D. L. Bryce, *Phys. Chem. Chem. Phys.* **2020**, *22*, 3817–3824.
[166] J. Vícha, J. Novotný, S. Komorovsky, M. Straka, M. Kaupp, R. Marek, *Chem. Rev.* **2020**, *120*, 7065–7103.
[167] M. Kaupp, in: *Theoretical and Computational Chemistry (Vol. 14: Relativistic Electronic Structure Theory. Part 2. Applications*), Ed. P. Schwerdtfeger, Elsevier, **2004**, pp. 552–597.
[168] I. L. Rusakova, Yu. Yu. Rusakov, *Magnetochemistry* **2023**, *9*, 24.
[169] I. L. Rusakova, L. B. Krivdin, *Mendeleev Commun.* **2018**, *28*, 1–13.

Manuscript received: September 19, 2023
Revised manuscript received: September 25, 2023
Accepted manuscript online: September 26, 2023
Version of record online: October 16, 2023